Letter

Manipulating vortices with domain walls in superconductor-ferromagnet heterostructures

Sebastián A. Díaz,[1,2] Jonas Nothhelfer,[1] Kjetil M. D. Hals,[3] and Karin Everschor-Sitte[1]
[1]*Faculty of Physics and Center for Nanointegration Duisburg-Essen (CENIDE), University of Duisburg-Essen, 47057 Duisburg, Germany*
[2]*Department of Physics, University of Konstanz, 78457 Konstanz, Germany*
[3]*Department of Engineering Sciences, University of Agder, NO-4879 Grimstad, Norway*

(Received 5 October 2023; accepted 24 April 2024; published 10 May 2024)

Vortices are pointlike topological defects in superconductors whose motion dictates superconducting properties and controls device performance. In superconductor-ferromagnet heterostructures, vortices interact with topological defects in the ferromagnet such as linelike domain walls. While in previous heterostructure generations, vortex-domain wall interactions were mediated by stray fields; in new heterostructure families, more important become exchange fields and spin-orbit coupling. However, spin-orbit coupling's role in vortex-domain wall interactions remains unexplored. Here we uncover, via numerical simulations and Ginzburg-Landau theory, that Rashba spin-orbit coupling induces magnetoelectric interactions between vortices and domain walls that crucially depend on the wall's winding direction—its helicity. The wall's helicity controls whether vortices are pushed or dragged by Néel walls, and their gliding direction along Bloch walls. Our work capitalizes on interactions between topological defects from different order parameters and of different dimensionality to engineer enhanced functionality.

DOI: 10.1103/PhysRevB.109.L201110

Introduction. Nature provides numerous examples where nanostructures of dissimilar kind and dimensionality work together to achieve specific functions: supramolecular capsules trap small molecules and act as catalytic centers [1,2], lipid bilayer membranes enclose organelles that determine cells' functionality [3], RNA polymerase glides along a DNA strand to transcribe genetic information [4,5]. In the spirit of these examples from Nature, topological defects of ordered media in condensed matter [6,7], such as pointlike skyrmions [8–12] and vortices [13–17], as well as linelike dislocations [18–21] and domain walls [22–25], have been actively investigated for technological applications. For instance, recent experiments have reported on skyrmion confinement using domain walls in liquid crystals and magnets [26,27]. Similarly, recent theoretical studies [28,29] and their experimental realization [30] have demonstrated guidance of magnetic skyrmions along tracks provided by the helical phase in helimagnets [31–33]. The main challenge faced by these recent reports was ensuring the coexistence of topological defects with different dimensionality and of the same order parameter [34].

An alternative to overcome this challenge and a path towards engineering enhanced functionality, as in the above examples from Nature, is to employ different order parameters: thus providing a much richer toolbox to manipulate individual and coupled structures. Progress has been made in superconductor-ferromagnet heterostructures [35–37], where magnetic domain walls interact with superconducting vortices via stray fields [38,39]. Moreover, the displacement [40,41] and confinement [42] of superconducting vortices by the stray field of magnetic domain walls have been experimentally demonstrated.

Current interest in proximity-coupled superconductor-magnet heterostructures stems from topological superconductivity [43–45] and the promise of realizing Majorana bound states [46,47] whose manipulation, for example, could be achieved via controlling magnetic skyrmions [48–51]. Spin-orbit coupling (SOC), necessary for topological superconductivity, is also present in heterostructures hosting superconducting vortices and magnetic domain walls, but its role has so far been neglected and remains unexplored.

Here we exploit the rich interplay between distinct order parameters in proximity-coupled superconductor-ferromagnet heterostructures, arising from the magnetoelectric effect induced by Rashba SOC [52–54], to manipulate superconducting vortices with magnetic domain walls (Fig. 1).

Textured ferromagnet proximity coupled to a superconductor. We assume the magnetic domain wall dynamics to

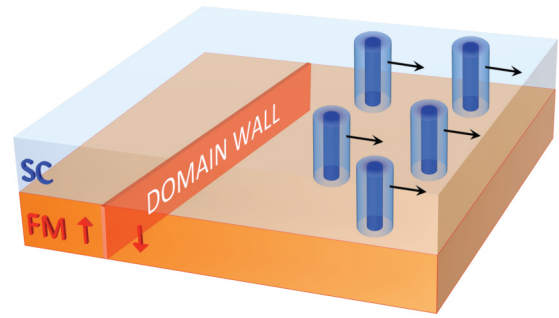

FIG. 1. Superconducting vortices manipulated by magnetic domain walls in superconductor-ferromagnet heterostructures. A domain wall in the ferromagnetic thin film (FM) that is proximity coupled to a superconducting layer (SC) interacts with vortices (blue tubes) via the magnetoelectric effect induced by spin-orbit coupling. The winding of the domain wall (helicity) and the vortices (vorticity) control whether vortices glide along the domain wall, get dragged, or (as depicted) pushed.

be externally controlled, for instance by in-plane magnetic fields [55,56] or temperature gradients [57–59], and aim to model its effect on the superconductor. The phenomena we are interested in possess a natural separation of timescales. While magnetic domain walls attain speeds of $\sim$10 μm/s when driven by in-plane magnetic fields [56] and of $\sim 10^2$ μm/s when driven by temperature gradients [59], itinerant electrons in clean superconductors are orders of magnitude faster due to typical Fermi velocities of $\sim 10^6$ m/s [60]. Therefore, we adopt an adiabatic approach where we simulate the time evolution of the superconducting order parameter as a sequence of static configuration steps. At each step, the magnetic texture in the proximity-coupled ferromagnet is a parameter set that modifies the electronic energy spectrum and eigenstates in the superconductor through the tight-binding Hamiltonian,

$$H = -t\sum_{\langle ij\rangle} \boldsymbol{c}_i^\dagger \boldsymbol{c}_j - \mu \sum_i \boldsymbol{c}_i^\dagger \boldsymbol{c}_i - \sum_i \boldsymbol{c}_i^\dagger (\boldsymbol{h}_i \cdot \boldsymbol{\sigma}) \boldsymbol{c}_i + \mathrm{i}\,\alpha_\mathrm{R} \sum_{\langle ij\rangle} \boldsymbol{c}_i^\dagger \hat{\boldsymbol{z}} \cdot (\hat{\boldsymbol{d}}_{ij} \times \boldsymbol{\sigma}) \boldsymbol{c}_j + \sum_i (\Delta_i c_{i\uparrow}^\dagger c_{i\downarrow}^\dagger + \mathrm{H.c.}). \tag{1}$$

Itinerant electrons of spin α are created (annihilated) at site i of the square lattice, on the xy plane and with lattice constant a, via the operator $c_{i\alpha}^\dagger (c_{i\alpha})$, and $\boldsymbol{c}_i = (c_{i\uparrow}, c_{i\downarrow})^T$. Here, t is the hopping parameter, μ is the chemical potential, and $\boldsymbol{h}_i$ is the exchange field due to the magnetic texture in the proximity-coupled ferromagnet. Rashba SOC enters through the fourth term, where α_R is the coupling strength, the unit vector $\hat{\boldsymbol{d}}_{ij}$ is oriented along the nearest-neighbor link from j to i, $\boldsymbol{\sigma}$ is the vector of Pauli matrices, and the coefficient i is the imaginary unit. Finally, Δ_i is the complex-valued and spatially dependent superconducting order parameter that we compute self-consistently (see [51] for details).

The above microscopic theory is valid for any magnetic texture; it was previously used to study pointlike skyrmions [61]. In this work, we consider domain walls whose linelike structure brings about new physics and functionality.

With this adiabatic and self-consistent model, we characterize the interactions between magnetic domain walls and superconducting vortices.

Vortex response to a moving domain wall. To reveal the interaction between a superconducting vortex and a magnetic domain wall, we simulate their adiabatic time evolution. The exchange field induced by the magnetic domain wall, aligned parallel to the y axis and centered at $x = 0$, reads

$$\boldsymbol{h}^{(dw)} = h_0[\sin\Theta(x)\,\hat{\boldsymbol{n}}^{(dw)}(\gamma) + \cos\Theta(x)\hat{\boldsymbol{z}}], \tag{2}$$

with h_0 the exchange field strength, $\hat{\boldsymbol{n}}^{(dw)}(\gamma) = \cos\gamma\,\hat{\boldsymbol{x}} + \sin\gamma\,\hat{\boldsymbol{y}}$, and γ the domain wall *helicity*. We choose $\boldsymbol{h}^{(dw)}$ pointing asymptotically upward (downward) to the domain wall's left (right): $\cos\Theta(x) = -\tanh(x/d)$, with d the domain wall width.

In the vortex vicinity, the superconducting order parameter phase becomes $\theta^{(v)} = q_v\phi + \varphi$. The winding number of $\theta^{(v)}$ about the vortex core, its *vorticity* q_v, and its *chirality* φ are determined by the background exchange field at the vortex and the Rashba SOC strength α_R. For concreteness, we focus on vortices with $q_v = 1$ [62].

We simulate four distinct helicity cases: Néel walls with $\gamma = 0, \pi$ and Bloch walls with $\gamma = \pi/2, 3\pi/2$ (see Supplemental Material [63]). Implementing a rigid, rightward domain wall motion yields strikingly different vortex responses.

A Néel wall with $\gamma = \pi$, when sufficiently close, constantly pushes the vortex to the right [Fig. 2(a), Neel-Push.mp4]. However, if the Néel wall has helicity $\gamma = 0$, a drastically different behavior occurs. The vortex is attracted towards the domain wall and eventually crosses to the left domain. Once in the domain wall's "wake," the vortex settles at a distance and the domain wall drags it [Fig. 2(b), Neel-Drag.mp4].

In contrast, Bloch walls initially attract the vortex. Once sufficiently close, the vortex chirality changes and the vortex motion acquires a vertical component. Eventually, the vortex gets trapped and then glides along the domain wall: for $\gamma = 3\pi/2$ in the $\hat{\boldsymbol{y}}$ direction [Fig. 2(c), Bloch-Glide-Up.mp4] and for $\gamma = \pi/2$ in the $-\hat{\boldsymbol{y}}$ direction [Fig. 2(d), Bloch-Glide-Down.mp4].

These diverse four cases admit a unified description, as we explain next, underpinned by the Rashba SOC-induced magnetoelectric effect [52–54].

Vortex-domain wall interactions. The numerical simulations presented above can be comprehended qualitatively through the Ginzburg-Landau theory of superconductors [64]. The spatially asymmetric Rashba SOC introduces coupling mechanisms between the superconducting condensate and the ferromagnetic layer, known as magnetoelectric interactions [52–54,61,65]. These interactions are incorporated into the Ginzburg-Landau phenomenology through the magnetoelectric free energy functional $F_{me}[\psi^*, \psi, \boldsymbol{A}, \boldsymbol{h}] = \int d\boldsymbol{r}\, \mathcal{F}_{me}^{(1)}$, where $\mathcal{F}_{me}^{(1)} = -\kappa^{(1)}(\hat{\boldsymbol{z}} \times \boldsymbol{h}) \cdot \boldsymbol{\mathcal{P}}$ is a SOC-induced Lifshitz invariant, and the positive constant $\kappa^{(1)}$ parameterizes the magnetoelectric coupling to first order in SOC [66]. Here, $\boldsymbol{h}$ is the exchange field induced in the superconductor by the adjacent ferromagnetic layer via the exchange proximity effect, $\boldsymbol{\mathcal{P}} = \mathrm{Re}[\psi^*(-\mathrm{i}\hbar\nabla - 2e\boldsymbol{A}/c)\psi]$ is the superconducting condensate's momentum density, $\psi(\boldsymbol{r}) = |\psi(\boldsymbol{r})| \exp[\mathrm{i}\theta(\boldsymbol{r})]$ is the superconductor's complex order parameter field, $2e$ ($e = -|e|$) is the charge of a Cooper pair, c is the speed of light, and $\boldsymbol{A}$ is the magnetic vector potential. We concentrate on a thin-film type-II superconductor where the magnetic field's penetration depth is significantly larger than the typical length scales that characterize spatial variations of magnetic domain walls and superconducting vortices; thus, we can disregard the magnetic vector potential [67]. An essential consequence of this magnetoelectric interaction is the emergence of the anomalous supercurrent density $\boldsymbol{j}_{as} = -2e|\psi|^2\kappa^{(1)}(\hat{\boldsymbol{z}} \times \boldsymbol{h})$ [63]. This is an additional contribution to the conventional supercurrent $\boldsymbol{j}_{cs} = e\boldsymbol{\mathcal{P}}/m$ generated by phase gradients in ψ, resulting in a net supercurrent density of $\boldsymbol{j}_s = \boldsymbol{j}_{cs} + \boldsymbol{j}_{as}$. Therefore, in proximity-coupled superconductor-ferromagnet heterostructures, textures with an in-plane component such as ferromagnetic domain walls produce anomalous supercurrents.

Incorporating the exchange field given by Eq. (2), we find the anomalous supercurrent density associated with a domain wall of general helicity $\boldsymbol{j}_{as}^{(dw)}(x, \gamma) = -g^{(1)}(x)\,\hat{\boldsymbol{z}} \times \hat{\boldsymbol{n}}^{(dw)}(\gamma)$, where $g^{(1)}(x) = \kappa^{(1)} 2eh_0|\psi|^2 \mathrm{sech}(x/d)$. While Néel walls

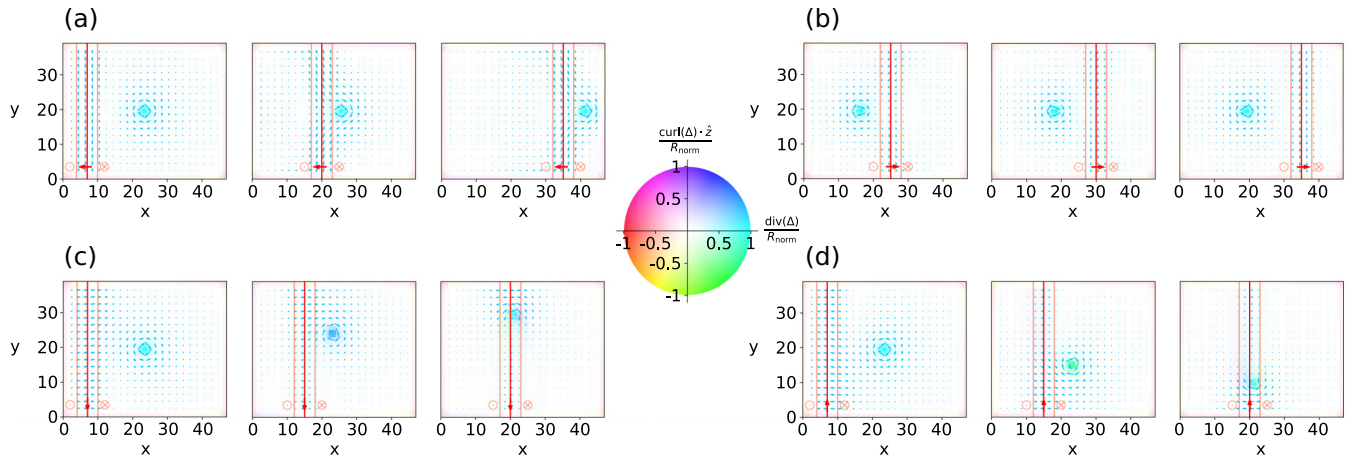

FIG. 2. Vortex response to a moving domain wall depends on helicity. Snapshots show the vortex time evolution in response to a rightward-moving domain wall (vertical red line) with helicity (red arrow): (a) $\gamma = \pi$, (b) $\gamma = 0$, (c) $\gamma = 3\pi/2$, and (d) $\gamma = \pi/2$. The superconducting order parameter is color coded (color wheel, normalization constant $R_{\text{norm}} = 0.75$) by its curl and divergence; lengths are in lattice constant a units; light blue arrows denote the supercurrent. A Néel wall with (a) $\gamma = \pi$ constantly pushes the vortex. In contrast, a Néel wall with (b) $\gamma = 0$ initially attracts the vortex, lets it move to the left domain, then drags it. After getting trapped by a Bloch wall, vortices glide along the wall in the $\hat{\boldsymbol{y}}$ direction for (c) $\gamma = 3\pi/2$ and in the $-\hat{\boldsymbol{y}}$ direction for (d) $\gamma = \pi/2$.

generate supercurrents along the wall, Bloch walls generate supercurrents across the wall.

On the other hand, a vortex centered at $\boldsymbol{R} = R_x\hat{\boldsymbol{x}} + R_y\hat{\boldsymbol{y}}$ can be characterized by the order parameter field $\psi^{(v)}(\boldsymbol{r}) = \psi_0 \tanh(|\boldsymbol{r} - \boldsymbol{R}|/\xi) \exp[i\theta^{(v)}(\boldsymbol{r})]$, where $\theta^{(v)}$ varies by 2π in making a complete circuit counterclockwise about the vortex center, ψ_0 denotes the order parameter's absolute value far from the vortex core, and ξ represents the coherence length [64]. This vortex profile generates the conventional supercurrent density $\boldsymbol{j}_{cs}^{(v)} = \frac{\hbar e \psi_0^2}{m} \frac{\tanh^2(|\boldsymbol{r}-\boldsymbol{R}|/\xi)}{|\boldsymbol{r}-\boldsymbol{R}|^2} \hat{\boldsymbol{z}} \times (\boldsymbol{r} - \boldsymbol{R})$, which is strongest when $|\boldsymbol{r} - \boldsymbol{R}| \sim \xi$ and approaches zero as $|\boldsymbol{r} - \boldsymbol{R}| \to 0$ and $|\boldsymbol{r} - \boldsymbol{R}| \to \infty$.

The vortex-domain wall magnetoelectric interactions are governed by the effective free energy $F_{\text{eff}}(\boldsymbol{R}, \gamma) = F_{me}[\psi^{(v)*}, \psi^{(v)}, \boldsymbol{h}^{(dw)}]$, which is obtained by substituting $\boldsymbol{h}^{(dw)}$, the exchange field of a domain wall with helicity γ given by Eq. (2), and $\psi^{(v)}$, the profile of a vortex centered at $\boldsymbol{R}$, into the magnetoelectric energy functional F_{me}, followed by integrating over the spatial coordinate $\boldsymbol{r}$. Through its dependence on $\boldsymbol{R}$ and γ, F_{eff} determines how the superconductor's free energy varies with the vortex's position relative to the domain wall.

We numerically compute the effective free energy, assuming the domain wall width and the coherence length are similar, $d \sim \xi$, in the vicinity of Néel [Fig. 3(a)] and Bloch [Fig. 3(b)] walls. For $\gamma = \pi$ ($\gamma = 0$) Néel walls, F_{eff} exhibits a global minimum at $R_x \sim \xi$ ($R_x \sim -\xi$) from the wall's center. This explains the simulation for $\gamma = \pi$ [Fig. 2(a)], where the vortex is pushed in front of the domain wall as it moves to the right, while for $\gamma = 0$ [Fig. 2(b)], the vortex crosses into the left domain and is dragged behind the moving wall. In contrast, for $\gamma = \pi/2$ ($\gamma = 3\pi/2$) Bloch walls, F_{eff} exhibits a global minimum at the end of the wall towards $-\hat{\boldsymbol{y}}$ ($+\hat{\boldsymbol{y}}$), where it intersects the sample boundary. Therefore, the effective free energy gives rise to a y component in the vortex

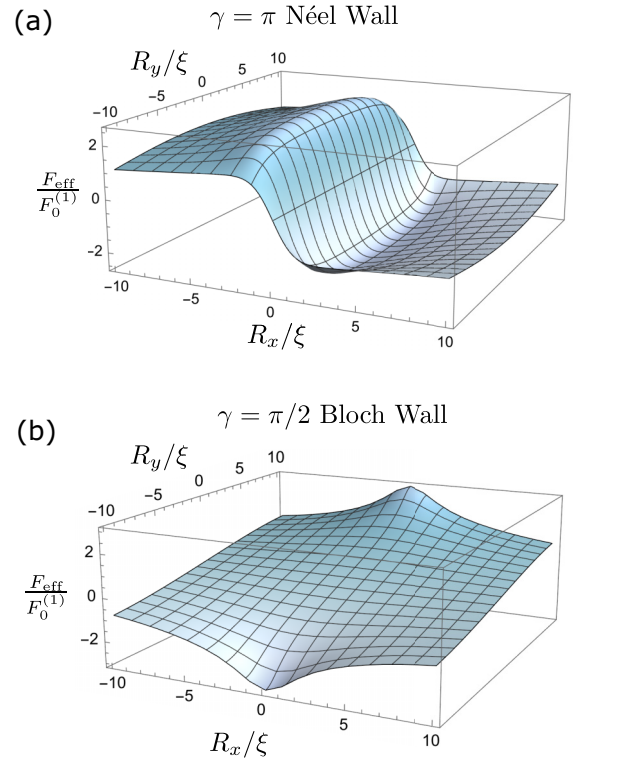

FIG. 3. Effective free energy landscapes: interacting vortex-domain wall. Minima of F_{eff}, with the domain wall fixed at $R_x = 0$, indicate the vortex equilibrium position. Parameters: sample size $[-\infty, +\infty] \times [-10\,\xi, 10\,\xi]$, domain wall width $d = 0.4\,\xi$, and $F_0^{(1)} = \kappa^{(1)} \pi \hbar\, d\, h_0 \psi_0^2$. (a) Néel wall with helicity $\gamma = \pi$: global minimum at $(R_x \sim \xi, R_y = 0)$, to the right of the wall's center, explains the simulation [Fig. 2(a)] where the wall pushes the vortex. (b) Bloch wall with helicity $\gamma = \pi/2$: global minimum at $(R_x = 0, R_y = -10\,\xi)$, at one of the wall ends on the sample boundary, explains the simulation [Fig. 2(d)] where the vortex glides along the wall.

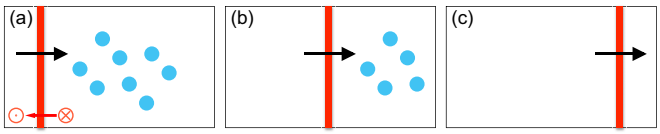

FIG. 4. Wiping the slate clean of superconducting vortices. Configurational sequence of a rightward-moving Néel wall with helicity $\gamma = \pi$ that pushes vortices away from the sample area, acting as a vortex "eraser" or "rake."

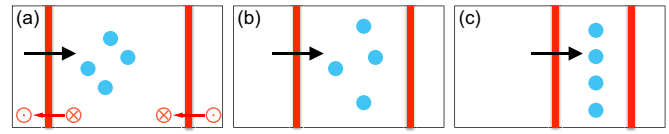

FIG. 5. Assembling a superconducting vortex chain using two magnetic domain walls. Configurational sequence of vortices confined between two Néel walls with helicity $\gamma = \pi$. As the separation between walls decreases, vortices rearrange (by wall pushing and repulsive vortex-vortex interactions) and form a chain.

motion [Figs. 2(c) and 2(d)], which explains its gliding along the wall.

Our analytical calculations [63] corroborate these numerical results and their helicity dependence. For Bloch walls, they also clearly show the removal of F_{eff}'s minima and maxima as the sample size approaches infinity—these minima and maxima are finite-size effects.

A simple physical picture of vortex-domain wall interactions follows from the interplay between anomalous and conventional supercurrents densities. When the superconductor-ferromagnet heterostructure contains a domain wall and a vortex, the superconductor aims to minimize its free energy by relocating the vortex to reduce the total supercurrent density $\boldsymbol{j}_s = \boldsymbol{j}_{cs}^{(v)} + \boldsymbol{j}_{as}^{(dw)}$ to a minimum [63]. For a Néel wall, the vortex reaches an equilibrium position at a distance $|R_x| \sim \xi$ from the wall's center because this ensures that the area with the strongest conventional supercurrent density around the vortex partly offsets the anomalous supercurrent density induced along the wall; while for Bloch walls, the vortex attains its equilibrium position at one of the wall ends to counteract the anomalous supercurrent density induced in the sample interior.

Exploiting these helicity-dependent vortex-domain wall interactions, in the following section we demonstrate practical routes to manipulate superconducting vortices with magnetic domain walls.

Manipulating vortices with domain walls. Vortex manipulation is relevant for technological applications. For instance, directional guidance of vortices underpins vortex-based logic platforms [51,68–70]. Additionally, confining vortices to narrow constrictions enhances vortex pinning, which extends the magnetic field range of the zero-resistance state [71] and improves the performance of superconducting electronic devices [72]. We employ the helicity-dependent vortex-domain wall interactions detailed in the previous sections to manipulate vortices with domain walls.

A Néel wall with helicity $\gamma = \pi$ pushes away and thus removes vortices from a specific sample area (Fig. 4, Vortex-Eraser.mp4). The same mechanism populates with vortices empty sample areas. Being mobile barriers, these domain walls can also suppress or trigger vortex avalanches [73–75].

Bloch walls, in finite-size setups, serve as unidirectional vortex channels where the wall's helicity controls the vortices propagation direction [Figs. 2(c) and 2(d)]. Alternatively, two Néel walls brought closer form a vortex channel; assisted by repulsive vortex-vortex interactions, they also assemble a vortex chain (Fig. 5, Vortex-Chain-Assembly.mp4). Although vortex chains have been reported before in anisotropic [76–78] and nanopatterned superconductors [72,79] and between twin boundaries [80], mobile magnetic domain walls represent an attractive noninvasive avenue to construct reconfigurable channels for vortices and vortex chains.

Our simulations demonstrate that exploiting the dependence on the wall's helicity of the vortex-domain wall interactions leads to enhanced functionality.

Discussion and conclusion. The experimental realization of our predictions requires superconductor-ferromagnet heterostructures where vortices and domain walls interact via Rashba SOC. The high-quality interfaces needed for Rashba SOC can be assembled using van der Waals (vdW) materials. For example, evidence of Rashba SOC has been reported at the interface of vdW ferromagnets and type-II superconductors: $Fe_{0.29}TaS_2/NbN$ [81] and $CrBr_3/NbSe_2$ [82]. Furthermore, $CrBr_3/NbSe_2$ supports vortices [83] and $CrBr_3$ hosts Bloch walls [84,85]. Gliding vortices along Bloch walls [Figs. 2(c) and 2(d)] we propose to observe in the existing $CrBr_3/NbSe_2$ heterostructure. Another vdW ferromagnet that exhibits Bloch walls is Fe_3GeTe_2 [86]; by decreasing its thickness or engineering its capping layer, Fe_3GeTe_2 can favor Néel walls [87,88]. Vortex pushing or dragging by Néel walls [Figs. 2(a) and 2(b)] we suggest to observe in $Fe_3GeTe_2/NbSe_2$ heterostructures. Therefore, superconductor-ferromagnet heterostructures suitable for the experimental realization of our predictions are available.

Conclusive experimental confirmation of our predictions needs tracking domain wall and vortex positions. Domain wall observation and helicity determination require measuring the magnetization's three components, achievable using spin-polarized scanning tunneling microscopy (SP-STM) [89], spin-polarized low-energy electron microscopy (SPLEEM) [90], or Lorentz transmission electron microscopy (TEM), even without sample tilting [91]. Additionally, note that our findings of helicity-dependent vortex-domain wall interactions provide an indirect method to measure the domain wall helicity. Vortex detection can be done via Lorentz TEM [92], magneto-optical imaging [39,40], magnetic force microscopy (MFM) [93,94], STM [95], and superconducting quantum interference device (SQUID) magnetometry [96]. Employment of a single technique to simultaneously image vortices and domain walls facilitates data collection and minimizes system disruption; this has been demonstrated using MFM [42]. There exist plenty of imaging techniques to confirm our predictions.

We have explained how Rashba spin-orbit coupling in superconductor-ferromagnet heterostructures induces interactions between superconducting vortices and magnetic domain

walls. Leveraging the dependence of these interactions on the domain walls' helicity, we have showcased enhanced functionalities that result from manipulating vortices with domain walls. The mobility of domain walls affords them a further advantage: repurposing the same sample by noninvasive reconfiguration of the magnetic landscape. Our work epitomizes Nature's paradigm of functionality via the interaction of dissimilar nanostructures, and embraces its extension to the condensed matter realm of topological defects of different order parameters and dimensionality.

Acknowledgments. We thank Stephan Kessler, Christos Panagopoulos, Danilo Nikolic, Michael Hein, and Wolfgang Belzig for helpful discussions. We thank Lucas Görzen for assistance in this work's preliminary stages. S.A.D. acknowledges funding by a Blue Sky project led by W. Belzig in the framework of the Excellence Strategy of the University of Konstanz. We acknowledge funding from the German Research Foundation (DFG) Project No. 320163632 (Emmy Noether), Project No. 403233384 (SPP2137 Skyrmionics), the Research Council of Norway via Project No. 334202, and support from the Max Planck Graduate Center. This research was supported in part by the National Science Foundation under Grant No. NSF PHY-1748958.

J.N. and S.A.D. contributed equally to this work.

[1] Q. Zhang and K. Tiefenbacher, Nat. Chem. **7**, 197 (2015).
[2] L.-D. Syntrivanis, I. Némethová, D. Schmid, S. Levi, A. Prescimone, F. Bissegger, D. T. Major, and K. Tiefenbacher, J. Am. Chem. Soc. **142**, 5894 (2020).
[3] B. Alberts, R. Heald, A. Johnson, D. Morgan, M. Raff, K. Roberts, and P. Walter, *Molecular Biology of the Cell* (W. W. Norton & Company, New York, 2022).
[4] T. I. Lee and R. A. Young, Ann. Rev. Genetics **34**, 77 (2000).
[5] Y. Suzuki, M. Shin, A. Yoshida, S. H. Yoshimura, and K. Takeyasu, FEBS Lett. **586**, 3187 (2012).
[6] N. D. Mermin, Rev. Mod. Phys. **51**, 591 (1979).
[7] P. Chaikin and T. Lubensky, *Principles of Condensed Matter Physics* (Cambridge University Press, Cambridge, 2000).
[8] S. Mühlbauer, B. Binz, F. Jonietz, C. Pfleiderer, A. Rosch, A. Neubauer, R. Georgii, and P. Böni, Science **323**, 915 (2009).
[9] X. Z. Yu, Y. Onose, N. Kanazawa, J. H. Park, J. H. Han, Y. Matsui, N. Nagaosa, and Y. Tokura, Nature (London) **465**, 901 (2010).
[10] A. N. Bogdanov, U. K. Rößler, and A. A. Shestakov, Phys. Rev. E **67**, 016602 (2003).
[11] K. Everschor-Sitte, J. Masell, R. M. Reeve, and M. Kläui, J. Appl. Phys. **124**, 240901 (2018).
[12] Y. Shen and I. Dierking, Phys. Rev. Appl. **15**, 054023 (2021).
[13] A. Hubert and R. Schäfer, *Magnetic Domains: The Analysis of Magnetic Microstructures* (Springer, Berlin, 1998).
[14] T. Shinjo, T. Okuno, R. Hassdorf, †. K. Shigeto, and T. Ono, Science **289**, 930 (2000).
[15] G. Blatter, M. V. Feigel'man, V. B. Geshkenbein, A. I. Larkin, and V. M. Vinokur, Rev. Mod. Phys. **66**, 1125 (1994).
[16] O. V. Lounasmaa and E. Thuneberg, Proc. Natl. Acad. Sci. USA **96**, 7760 (1999).
[17] M. M. Salomaa and G. E. Volovik, Rev. Mod. Phys. **59**, 533 (1987).
[18] D. Hull and D. Bacon, *Introduction to Dislocations* (Elsevier, Amsterdam, 2011).
[19] M. Kleman, Rep. Prog. Phys. **52**, 555 (1989).
[20] P. Schoenherr, J. Müller, L. Köhler, A. Rosch, N. Kanazawa, Y. Tokura, M. Garst, and D. Meier, Nat. Phys. **14**, 465 (2018).
[21] M. Azhar, V. P. Kravchuk, and M. Garst, Phys. Rev. Lett. **128**, 157204 (2022).
[22] A. P. Malozemoff and J. C. Slonczewski, *Magnetic Domain Walls in Bubble Materials* (Elsevier, Amsterdam, 1979).
[23] D. Meier, J. Seidel, M. Gregg, and R. Ramesh, *Domain Walls: From Fundamental Properties to Nanotechnology Concepts* (Oxford University Press, Oxford, 2020).
[24] G. F. Nataf, M. Guennou, J. M. Gregg, D. Meier, J. Hlinka, E. K. H. Salje, and J. Kreisel, Nat. Rev. Phys. **2**, 634 (2020).
[25] D. Meier and S. M. Selbach, Nat. Rev. Mater. **7**, 157 (2021).
[26] D. Foster, C. Kind, P. J. Ackerman, J.-S. B. Tai, M. R. Dennis, and I. I. Smalyukh, Nat. Phys. **15**, 655 (2019).
[27] J. Tang, Y. Wu, W. Wang, L. Kong, B. Lv, W. Wei, J. Zang, M. Tian, and H. Du, Nat. Nanotechnol. **16**, 1086 (2021).
[28] R. Knapman, D. R. Rodrigues, J. Masell, and K. Everschor-Sitte, J. Phys. D **54**, 404003 (2021).
[29] L. Kong, X. Chen, W. Wang, D. Song, and H. Du, Phys. Rev. B **104**, 214407 (2021).
[30] D. Song, W. Wang, J.-X. Yu, P. Zhang, S. S. Pershoguba, G. Yin, W. Wei, J. Jiang, B. Ge, X. Fan, M. Tian, A. Rosch, J. Zang, and H. Du, arXiv:2212.08991.
[31] M. Ezawa, Phys. Rev. B **83**, 100408(R) (2011).
[32] J. Müller, J. Rajeswari, P. Huang, Y. Murooka, H. M. Rønnow, F. Carbone, and A. Rosch, Phys. Rev. Lett. **119**, 137201 (2017).
[33] M. Stepanova, J. Masell, E. Lysne, P. Schoenherr, L. Köhler, M. Paulsen, A. Qaiumzadeh, N. Kanazawa, A. Rosch, Y. Tokura, A. Brataas, M. Garst, and D. Meier, Nano Lett. **22**, 14 (2022).
[34] Realizing the coexistence of topological defects with different dimensionality within the same order parameter is indeed a challenging experimental task: it requires careful sample fabrication design and precise topological defect nucleation and control protocols [30].
[35] I. F. Lyuksyutov and V. L. Pokrovsky, Adv. Phys. **54**, 67 (2005).
[36] A. I. Buzdin, Rev. Mod. Phys. **77**, 935 (2005).
[37] A. Y. Aladyshkin, A. V. Silhanek, W. Gillijns, and V. V. Moshchalkov, Supercond. Sci. Technol. **22**, 053001 (2009).
[38] L. E. Helseth, P. E. Goa, H. Hauglin, M. Baziljevich, and T. H. Johansen, Phys. Rev. B **65**, 132514 (2002).
[39] J. I. Vestgarden, D. V. Shantsev, A. A. F. Olsen, Y. M. Galperin, V. V. Yurchenko, P. E. Goa, and T. H. Johansen, Phys. Rev. Lett. **98**, 117002 (2007).
[40] P. E. Goa, H. Hauglin, A. A. F. Olsen, D. Shantsev, and T. H. Johansen, Appl. Phys. Lett. **82**, 79 (2003).
[41] V. Vlasko-Vlasov, U. Welp, G. Karapetrov, V. Novosad, D. Rosenmann, M. Iavarone, A. Belkin, and W.-K. Kwok, Phys. Rev. B **77**, 134518 (2008).
[42] M. Iavarone, A. Scarfato, F. Bobba, M. Longobardi, G. Karapetrov, V. Novosad, V. Yefremenko, F. Giubileo, and A. M. Cucolo, Phys. Rev. B **84**, 024506 (2011).
[43] L. Fu and C. L. Kane, Phys. Rev. Lett. **100**, 096407 (2008).
[44] R. M. Lutchyn, J. D. Sau, and S. Das Sarma, Phys. Rev. Lett. **105**, 077001 (2010).

[45] Y. Oreg, G. Refael, and F. von Oppen, Phys. Rev. Lett. **105**, 177002 (2010).

[46] A. Y. Kitaev, Phys. Usp. **44**, 131 (2001).

[47] J. Alicea, Rep. Prog. Phys. **75**, 076501 (2012).

[48] J. Nothhelfer, K. M. D. Hals, K. Everschor-Sitte, and M. Rizzi, European Patent Application EP3751472A1/International Patent Application WO2020249630A1 and Pending Patent CN114008639A (pending).

[49] J. Nothhelfer, Master's thesis, Johannes Gutenberg University Mainz, 2019.

[50] S. A. Díaz, J. Klinovaja, D. Loss, and S. Hoffman, Phys. Rev. B **104**, 214501 (2021).

[51] J. Nothhelfer, S. A. Díaz, S. Kessler, T. Meng, M. Rizzi, K. M. D. Hals, and K. Everschor-Sitte, Phys. Rev. B **105**, 224509 (2022).

[52] V. M. Edelstein, Phys. Rev. Lett. **75**, 2004 (1995).

[53] V. M. Edelstein, J. Phys.: Condens. Matter **8**, 339 (1996).

[54] S. K. Yip, Phys. Rev. B **65**, 144508 (2002).

[55] T. Fang and A. Thiele, IEEE Trans. Magn. **26**, 1524 (1990).

[56] Y. P. Kabanov, Y. L. Iunin, V. I. Nikitenko, A. J. Shapiro, R. D. Shull, L. Y. Zhu, and C. L. Chien, IEEE Trans. Magnet. **46**, 2220 (2010).

[57] L. Berger, J. Appl. Phys. **58**, 450 (1985).

[58] J. Torrejon, G. Malinowski, M. Pelloux, R. Weil, A. Thiaville, J. Curiale, D. Lacour, F. Montaigne, and M. Hehn, Phys. Rev. Lett. **109**, 106601 (2012).

[59] W. Jiang, P. Upadhyaya, Y. Fan, J. Zhao, M. Wang, L.-T. Chang, M. Lang, K. L. Wong, M. Lewis, Y.-T. Lin, J. Tang, S. Cherepov, X. Zhou, Y. Tserkovnyak, R. N. Schwartz, and K. L. Wang, Phys. Rev. Lett. **110**, 177202 (2013).

[60] N. W. Ashcroft and N. D. Mermin, *Solid State Physics* (Holt, Rinehart and Winston, New York, 1976).

[61] K. M. D. Hals, M. Schecter, and M. S. Rudner, Phys. Rev. Lett. **117**, 017001 (2016).

[62] We do so by identifying model parameters that make a $q_v = 1$ vortex, in a field polarized magnetic background, the lowest-energy topologically nontrivial configuration of the superconducting order parameter.

[63] See Supplemental Material at http://link.aps.org/supplemental/10.1103/PhysRevB.109.L201110 for details as well as videos of the vortex and domain wall simulations, Ginzburg-Landau theory, effective free energy, magnetoelectric effect to second order in SOC, which includes Ref. [97].

[64] M. Tinkham, *Introduction to Superconductivity* (Dover, New York, 1996).

[65] S. S. Pershoguba, K. Björnson, A. M. Black-Schaffer, and A. V. Balatsky, Phys. Rev. Lett. **115**, 116602 (2015).

[66] The contribution to the magnetoelectric coupling to second order in the SOC, as our calculations in [63] show, is negligible.

[67] N. Kopnin, *Theory of Nonequilibrium Superconductivity* (Oxford University Press, Oxford, 2001), p. 238.

[68] K. Nakajima, Y. Onodera, and Y. Ogawa, J. Appl. Phys. **47**, 1620 (1976).

[69] C. O. Reichhardt, C. Reichhardt, M. Hastings, and B. Jankó, Phys. C: Superconduct. **404**, 266 (2004).

[70] I. Keren, A. Gutfreund, A. Noah, N. Fridman, A. D. Bernardo, H. Steinberg, and Y. Anahory, Nano Lett. **23**, 4669 (2023).

[71] R. Córdoba, T. I. Baturina, J. Sesé, A. Y. Mironov, J. M. D. Teresa, M. R. Ibarra, D. A. Nasimov, A. K. Gutakovskii, A. V. Latyshev, I. Guillamón, H. Suderow, S. Vieira, M. R. Baklanov, J. J. Palacios, and V. M. Vinokur, Nat. Commun. **4**, 1437 (2013).

[72] O. V. Dobrovolskiy, Phys. C: Superconduct. Applic. **533**, 80 (2017).

[73] S. Field, J. Witt, F. Nori, and X. Ling, Phys. Rev. Lett. **74**, 1206 (1995).

[74] E. Altshuler and T. H. Johansen, Rev. Mod. Phys. **76**, 471 (2004).

[75] F. Laviano, in *Vortices and Nanostructured Superconductors*, edited by A. Crisan (Springer International, Cham, Switzerland, 2017), pp. 133–157.

[76] T. Matsuda, O. Kamimura, H. Kasai, K. Harada, T. Yoshida, T. Akashi, A. Tonomura, Y. Nakayama, J. Shimoyama, K. Kishio, T. Hanaguri, and K. Kitazawa, Science **294**, 2136 (2001).

[77] A. Grigorenko, S. Bending, T. Tamegai, S. Ooi, and M. Henini, Nature (London) **414**, 728 (2001).

[78] S. J. Bending and M. J. W. Dodgson, J. Phys.: Condens. Matter **17**, R955 (2005).

[79] R. Córdoba, P. Orús, Ž. L. Jelić, J. Sesé, M. R. Ibarra, I. Guillamón, S. Vieira, J. J. Palacios, H. Suderow, M. V. Milosević, and J. M. D. Teresa, Sci. Rep. **9**, 41598 (2019).

[80] S. Y. Song, C. Hua, L. Bell, W. Ko, H. Fangohr, J. Yan, G. B. Halász, E. F. Dumitrescu, B. J. Lawrie, and P. Maksymovych, Nano Lett. **23**, 2822 (2023).

[81] R. Cai, Y. Yao, P. Lv, Y. Ma, W. Xing, B. Li, Y. Ji, H. Zhou, C. Shen, S. Jia, X. C. Xie, I. Žutić, Q.-F. Sun, and W. Han, Nat. Commun. **12**, 41467 (2021).

[82] S. Kezilebieke, M. N. Huda, V. Vaňo, M. Aapro, S. C. Ganguli, O. J. Silveira, S. Głodzik, A. S. Foster, T. Ojanen, and P. Liljeroth, Nature (London) **588**, 424 (2020).

[83] S. Kezilebieke, V. Vaňo, M. N. Huda, M. Aapro, S. C. Ganguli, P. Liljeroth, and J. L. Lado, Nano Lett. **22**, 328 (2022).

[84] V. R. Matricardi, W. G. Lehmann, N. Kitamura, and J. Silcox, J. Appl. Phys. **38**, 1297 (1967).

[85] Q.-C. Sun, T. Song, E. Anderson, A. Brunner, J. Förster, T. Shalomayeva, T. Taniguchi, K. Watanabe, J. Gräfe, R. Stöhr, X. Xu, and J. Wrachtrup, Nat. Commun. **12**, 41467 (2021).

[86] H.-H. Yang, N. Bansal, P. Rüßmann, M. Hoffmann, L. Zhang, D. Go, Q. Li, A.-A. Haghighirad, K. Sen, S. Blügel, M. L. Tacon, Y. Mokrousov, and W. Wulfhekel, 2D Mater. **9**, 025022 (2022).

[87] M. T. Birch, L. Powalla, S. Wintz, O. Hovorka, K. Litzius, J. C. Loudon, L. A. Turnbull, V. Nehruji, K. Son, C. Bubeck, T. G. Rauch, M. Weigand, E. Goering, M. Burghard, and G. Schütz, Nat. Commun. **13**, 41467 (2022).

[88] L. Peng, F. S. Yasin, T.-E. Park, S. J. Kim, X. Zhang, T. Nagai, K. Kimoto, S. Woo, and X. Yu, Adv. Funct. Mater. **31**, 2103583 (2021).

[89] M. Bode, M. Heide, K. von Bergmann, P. Ferriani, S. Heinze, G. Bihlmayer, A. Kubetzka, O. Pietzsch, S. Blügel, and R. Wiesendanger, Nature (London) **447**, 190 (2007).

[90] G. Chen and A. K. Schmid, Adv. Mater. **27**, 5738 (2015).

[91] J. J. Chess, S. A. Montoya, E. E. Fullerton, and B. J. McMorran, AIP Adv. **7**, 056807 (2017).

[92] K. Harada, T. Matsuda, J. Bonevich, M. Igarashi, S. Kondo, G. Pozzi, U. Kawabe, and A. Tonomura, Nature (London) **360**, 51 (1992).

[93] A. Moser, H. J. Hug, I. Parashikov, B. Stiefel, O. Fritz, H. Thomas, A. Baratoff, H.-J. Güntherodt, and P. Chaudhari, Phys. Rev. Lett. **74**, 1847 (1995).

[94] O. M. Auslaender, L. Luan, E. W. J. Straver, J. E. Hoffman, N. C. Koshnick, E. Zeldov, D. A. Bonn, R. Liang, W. N. Hardy, and K. A. Moler, Nat. Phys. **5**, 35 (2009).

[95] H. F. Hess, R. B. Robinson, R. C. Dynes, J. M. Valles, and J. V. Waszczak, Phys. Rev. Lett. **62**, 214 (1989).

[96] L. Embon, Y. Anahory, Ž. Jelić, E. O. Lachman, Y. Myasoedov, M. E. Huber, G. P. Mikitik, A. V. Silhanek, M. V. Milošević, A. Gurevich, and E. Zeldov, Nat. Commun. **8**, 85 (2017).

[97] K. M. D. Hals, Phys. Rev. B **93**, 115431 (2016).